High-Order Harmonic Generation in Solids: The Role of Intraband Transitions in Extreme Nonlinear Optics

Hideki Hirori[1,*], *Shunsuke A. Sato*[2,3,*], *and Yoshihiko Kanemitsu*[1,*]

[1]Institute for Chemical Research, Kyoto University, Uji, Kyoto 611-0011, Japan

[2]Center for Computational Sciences, University of Tsukuba, Tsukuba 305-8577, Japan

[3]Max Planck Institute for the Structure and Dynamics of Matter, Luruper Chaussee 149, 22761 Hamburg, Germany

*Corresponding Authors: hirori@scl.kyoto-u.ac.jp (Hideki Hirori), ssato@ccs.tsukuba.ac.jp (Shunsuke A. Sato), kanemitu@scl.kyoto-u.ac.jp (Yoshihiko Kanemitsu)

Keywords: High-order harmonic generation, Nonlinear optics, Nano materials, Optical transitions, Lightwave electronics

ABSTRACT

High-order harmonic generation (HHG) in gases is frequently used nowadays to produce attosecond pulses and coherent radiation in the visible-to-soft-X-ray spectral range. HHG in solids is a natural extension of idea of HHG in gases, and its first observation about ten years ago opened the door to investigations on attosecond electron dynamics in solids and the development of solid-state attosecond light sources. The common process in both types of HHG is nonlinear photocarrier generation, and thus transitions between different bands (interband transitions) are always important for HHG. As well, in the case of solids, the transitions within a band (intraband transitions) also need to be considered, because efficient carrier acceleration is possible due to them. This perspective focuses on experimental findings that show how intraband transitions can be controlled, because such an understanding will be essential in the development of unique optoelectronics that can operate at petahertz frequencies.

TOC graphic

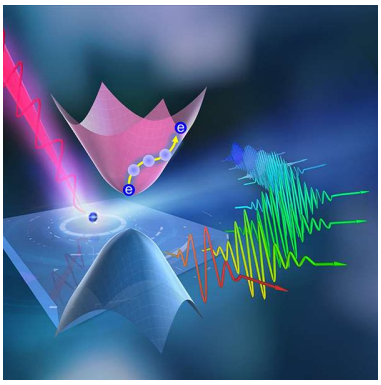

The field of nonlinear optics began to receive significant attention soon after the first demonstration of the laser, and in the course of time, it has seen various technological developments.[1,2] For example, it has been shown that strong excitations of atoms or molecules can induce emissions of so-called high-order harmonics, i.e., radiation that contains photons with energies that are integer multiples of the photon energy used for excitation.[3] The emitted light is thus said to consist of different orders. This phenomenon of high-order harmonic generation (HHG) in atomic and molecular systems has already been applied to attosecond-pulse and coherent keV-X-ray generation as well as to observation and manipulation of ultrafast electron dynamics.[4–6] The discovery of HHG in atomic and molecular systems has had a substantial impact on science, and the pioneering work on this topic was honored with the Nobel Prize for Physics in 2023. Strong-field physics in solids, however, is not so straightforward to study, because the strong excitation conditions required for HHG usually damage the material. Thus, non-resonant excitation is required, which means that we need laser light in the terahertz or midinfrared range,[7–16] depending on the chosen solid. Fortunately, the development of intense laser sources in the terahertz and mid-infrared frequency regions has enabled us to apply low-frequency electric fields with intensities comparable to the critical field strength (the strength of the atomic potential; a few volts per nanometer). The first report on HHG in bulk crystals with sub-bandgap emission was published about two decades ago, and its experimental results were explained in terms of a process in the perturbative regime.[17] About ten years later, non-perturbative HHG spectra of ZnO[18] (shown in Figure 1a) and GaSe[19] (shown in Figure 1b) were reported. This accelerated the progress of research on HHG in solids, as non-perturbative HHG enables pulses in the extreme-ultraviolet spectral range to be generated.[20–24]

The semiclassical three-step model for HHG, which was developed in the early 1990s, is able to explain the most important characteristics of HHG in gases: It describes the initial tunneling ionization of an electron, the following acceleration, and the final recollision process of the electron with the parent ion.[25–27] For a quantitative explanation of HHG in solids, however, more complex models are required. Even before the discovery of non-perturbative HHG in solids, theoretical discussions had already pointed out a potential enhancement through carrier acceleration.[25] Regarding HHG in crystals, coherent transitions between the valence and conduction bands (interband transitions) and the nonlinear current generated by acceleration of carriers in a band of the crystal (intraband transitions) need to be considered (Figure 2a): The microscopic picture here is photocarrier generation followed by acceleration of electrons in the first Brillouin zone and eventual electron–hole recombination, which leads to HHG (i.e., both acceleration and recombination can lead to HHG). In particular, the efficient increase of ponderomotive energy by an intense low-frequency field implies efficient carrier acceleration and thus emphasizes the impact of intraband transition processes in solids.[28–31] Note that the term intraband transition refers to the shift of the momentum of carriers as described in Figure 2a, and it is also known as the intraband motion. The nonlinear coupling between the interband and intraband transitions modifies the carrier generation process as schematically shown in Figure 2b, and depending on the material and the driving field, the carrier generation efficiency may increase or also decrease due to coupling.[32] Furthermore, the dynamical Bloch oscillations that occur when the electrons reach the boundary of the Brillouin zone also contribute to HHG (dynamical Bloch oscillations in a crystal with a multiband structure can lead to an HHG spectrum that contains a second plateau, as shown in Figure 1b).[19] Thus, besides its provision of attosecond light sources,

HHG is also useful for optically characterizing electronic states across the entire Brillouin zone in solids, leading to the idea of all-optical reconstruction of the band structure.[33–36]

We consider that the role of intraband transitions in HHG should receive more attention in the context of lightwave electronics, which refers to the idea of controlling electrons using very short (sub-cycle) light pulses.[37–44] However, while the importance of intraband transitions for efficient HHG in solids is widely accepted, experimental approaches that can separate the contributions from the interband- and intraband-transitions are rare. Recent observation of HHG from nanocrystals provided new insights into understanding of the intraband transitions in solids.[45,46] In this perspective, we introduce our recent experimental and theoretical work on intraband transitions to discuss how these transitions affect the HHG intensity and how these transitions can be controlled by nanosizing (e.g. use of quantum dots or graphene) or also by using two-color laser fields.[45–48] These insights should be useful for making technological advances, because the understanding and control of intraband transitions will be essential for the development of lightwave electronics and for all-optical reconstruction of the band structures of various materials.

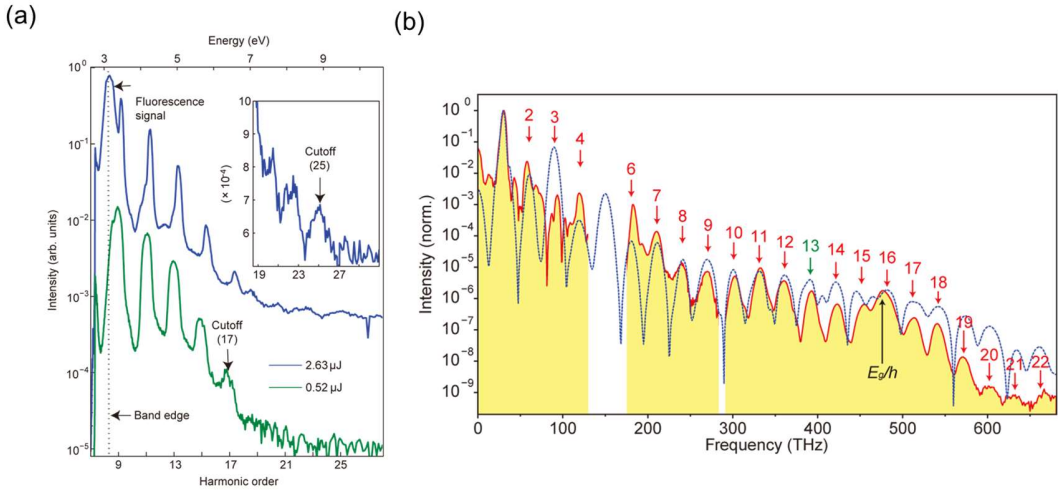

Figure 1. (a) HHG spectra of ZnO for different excitation intensities (excitation photon: 0.38 eV). Only odd harmonic orders are observed in this experiment due to inversion symmetry. (b) HHG spectrum of GaSe excited by a short terahertz pulse with a peak electric field of 72 MV/cm. Here, even- and odd-order harmonics can be observed. A second plateau is observed in the frequency range of 200-500 THz. Panel (a) is reproduced with permission from Ref. 18. Copyright 2011, Springer Nature. Panel (b) is reproduced with permission from Ref. 19. Copyright 2014, Springer Nature.

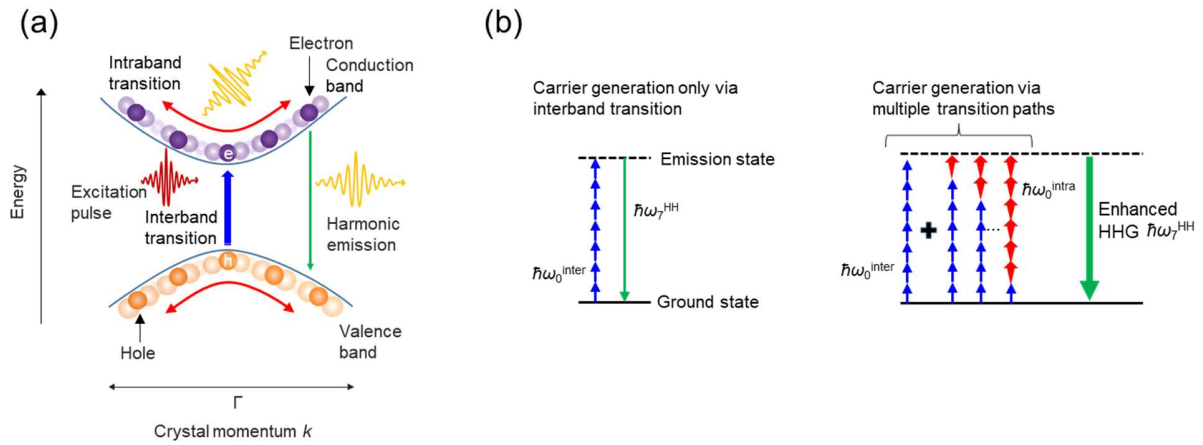

Figure 2. (a) Schematic diagram of the different processes during HHG. (b) Coupling of intraband and interband transitions enhancing HHG. In addition to the contribution of the pure interband transition terms (left), the efficient intraband transition in a larger bulk crystal opens up multiple excitation paths due to the nonlinear coupling between the intra- and interband transitions (right). At least in several direct-gap semiconductors, the additional excitation channels induced by the combination of intraband and interband transitions can enhance nonlinear carrier injection and thus also enhance HHG (Refs. 19, 31, 46).

HHG in solids is a rather complex phenomenon since various radiation mechanisms are possible.[49–51] In general, the electric current $J(t)$ in a crystal contains both interband- and intraband contributions. The power spectrum of HHG can be evaluated from $J(t)$ because the emission of harmonics is related to the acceleration of charged particles. Therefore, an analysis of the current corresponds to an analysis of the photon emission process. On the other hand, the intraband and interband transitions due to a given light field directly specify the driving process. Therefore, an analysis of the intraband and interband transitions is useful for identifying the radiation mechanism (SI Section 1).

Under adiabatic conditions, the acceleration of an electron in a band constitutes an intraband transition with a wavevector shift: $\boldsymbol{k} \rightarrow \boldsymbol{k} + e\boldsymbol{A}(t)/\hbar$,[28] where $\boldsymbol{k}$ is the Bloch wavevector of the considered Bloch state and $\boldsymbol{A}(t)$ is a spatially uniform vector potential that is related to the external electric field $\boldsymbol{E}(t)$ according to $\boldsymbol{A}(t) = -\int^t dt'\, \boldsymbol{E}(t')$. Depending on the rate of change in $\boldsymbol{k}$, two regimes can be considered: conventional optics and extreme nonlinear optics. In the former regime (resonant or near-resonant excitation conditions), typically only a small shift $\Delta\boldsymbol{k}$ can be reached due to the extremely short optical cycle-period oscillation of the excitation light, leading to a dominant contribution from the interband transitions between the valence band and the conduction band. In the latter regime (non-resonant condition), where usually terahertz or mid-infrared pulses are used, the wavevector shift tends to reach large values due to the relatively slow oscillation of the excitation light, and thus intraband transitions play a major role in the optically induced dynamics. Furthermore, the nonlinear coupling between the interband and intraband transitions should modify the carrier generation process. However, it is not always easy to separate the contributions of these transitions. Fortunately, the nature of the electronic bands of quantum dots (QDs) can be utilized to assess the role of intraband transitions,[52–55] because they can be

continuously tuned from atom-like discrete states to a band continuum.[45,46,56,57] Our first observation of HHG from perovskite QDs implied that QDs can be used to study the intraband transition effects on HHG.[45]

In the following, we consider small QDs made of CdSe, which has a bandgap energy of 1.75 eV. In the case of strong quantum confinement, the transition energies between different subbands are on the order of hundreds of millielectronvolt. Figure 3a shows the HHG spectra of different CdSe QD films for an excitation with linearly polarized mid-infrared light (photon energy: 0.35 eV). The pulse duration was 80 fs and the maximum electric field strength was 19 MV/cm. We find that the peak intensities increase as the average QD diameter increases (as the quantum confinement becomes weaker), and the strongest increase is observed in the range from 2 to 3 nm. These features are related to intraband transitions. In CdSe, the accelerated electrons mainly contribute to HHG, because the effective electron mass is significantly smaller than the effective hole mass ($m_e^*/m_h^* > 3$), and the estimated path length [$L = eET^2/(2\pi^2 m_e^*)$ of the electron (e is the elementary charge)] is about 15 nm during one half optical cycle T of the excitation field E = 20 MV/cm, $T = 1.2\times10^{-14}$ s, and $m_e^* = 0.13\ m_0$. The change in the spatial confinement caused by increasing the QD size is thus important for interpreting the observed data. Furthermore, we need to consider that the spatial confinement is directly related to the energy spacing between the confined electron states.

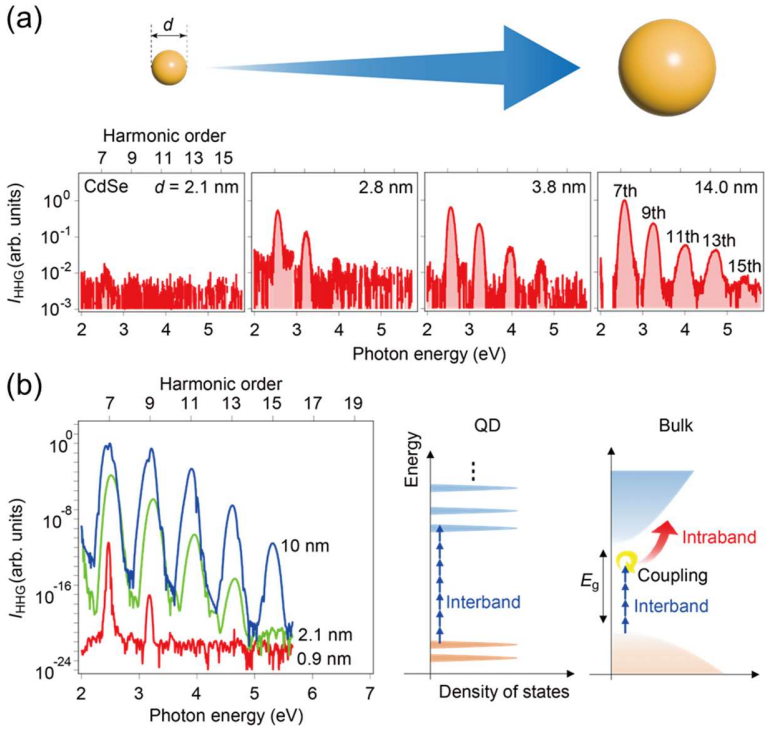

Figure 3. (a) QD-size dependence of the HHG spectrum of a CdSe QD film. (b) Numerical prediction of the QD-size dependence of the HHG spectrum based on a one-dimensional dimer chain model (left panel) and schematic excitation processes without (center panel) and with coupling between intraband and interband transitions (right panel). The figures are adapted with permission from Ref. 46. Copyright 2022, The Authors, under exclusive license to Springer Nature.

The effect of intraband transitions on the QD-size dependence of HHG can be explained by considering the electron dynamics in a simple one-dimensional dimer chain model. Figure 3b shows the computed HHG spectra for different QD diameters (chain lengths). By changing the calculation conditions, it can be verified that weaker quantum confinement of the electron (a longer chain) leads to stronger HHG. A change in the size of the QD changes both the lowest electron–

hole transition energy (the QD bandgap) and the intraband transitions energies between the confined electron states. Although the narrowing of the bandgap caused by the longer chain does not have a significant impact on the diameter dependence of HHG, the contribution from the intraband transitions in the case of a longer chain is significant. This behavior can be explained by the fact that HHG is a coherent optical process where a superposition of multiple transitions from various microscopic paths occurs due to the nonlinear coupling between the intra- and interband transitions. An understanding of this coupling process, which is discussed in the next section, together with our findings on the control of nonlinear optical phenomena by nanosizing are important considerations for the development of lightwave electronics, especially nanoscale devices.

The experiment in the previous paragraphs clarified that intraband transitions can significantly enhance HHG in solids. In this section, we theoretically explore the role of intraband transitions in HHG from the viewpoint of the coupling with interband transitions. In particular, we shall investigate HHG in graphene, since this material has a distinct ellipticity dependence to its HHG yield,[58] which can be attributed to its Dirac cone dispersion.[59–61] Optically induced Dirac-cone intraband and interband transitions are schematically described in Figure 4a. These transitions cause different types of perturbation of the electronic state. Multi-photon processes can be described by a combination of intraband and interband transitions, as shown in Figure 4b.

To clarify the microscopic origin of the ellipticity dependence of HHG in graphene, we performed a numerical simulation of the electron dynamics by using a quantum master-equation approach and compared its results with experimental results.[47] Figure 4c shows that the simulation reproduces the experimentally observed behavior: an enhanced HHG yield in the case of a larger

ellipticity. Additionally, we performed a simulation that only allows intraband transitions (Figure 4d; red dashed curve) and a simulation that only allows interband transitions (Figure 4d; blue dotted curve). Since neither the pure-intraband case nor the pure-interband case can explain the observed enhancement of HHG, the coupling of these transitions plays an essential role.

As mentioned in the previous section, the intraband transitions can be described by a wavevector shift $\boldsymbol{k} \rightarrow \boldsymbol{k} + e\boldsymbol{A}(t)/\hbar$ (SI Section 1). The interband transitions can be described in terms of the dipole matrix element (denoted by $\tilde{\boldsymbol{d}}_{bb'\boldsymbol{k}}(t)$) and the electric field $\boldsymbol{E}(t)$. Considering the contribution from the dynamical phase factor in the adiabatic solution of the Schrödinger equation for independent electrons, the magnitude of the intraband transitions can be estimated by using the slope of the band, $\frac{\partial}{\partial \boldsymbol{k}} \epsilon_{b\boldsymbol{k}}$, where $\epsilon_{b\boldsymbol{k}}$ is the eigenvalue of the Hamiltonian. The magnitude of the interband transitions can be directly evaluated using $\tilde{\boldsymbol{d}}_{bb'\boldsymbol{k}}(t)$. Figures 4e–4h show $\frac{\partial}{\partial \boldsymbol{k}} \epsilon_{b\boldsymbol{k}}$ and $\tilde{\boldsymbol{d}}_{bb'\boldsymbol{k}}(t)$ in the Brillouin zone with respect to both directions of the two-dimensional layer (the *x* and *y* directions). The Dirac cone of graphene is located at the origin. As can be seen from Figures 4e and 4g, the distributions of the intraband transitions are particularly strong along the x- and y-axes, respectively. On the other hand, the distributions of the interband transitions are particularly strong along the y- and x-axes, respectively (Figures 4f and 4h). Therefore, in the case of linearly polarized light, the intra- and interband distributions hardly overlap in the Brillouin zone, and thus, the coupling between them is not very effective. The observed distributions imply that more efficient coupling should occur in the case of elliptically polarized light, which is in agreement with the experiments. This confirms that the cross coupling between the intraband and interband transitions plays a central role in enhancing HHG. This result further indicates that the coupling between intraband and interband transitions is also important for HHG in various other solids.

In a similar way, the results on QDs can be interpreted in terms of coupling: The contribution to intraband-transition-induced radiation from the coupling increases if the intraband transitions are enhanced by using larger QDs. Our results indicate that the primary impact of intraband transitions in these types of solids is a more efficient nonlinear carrier generation, and this results in stronger HHG.

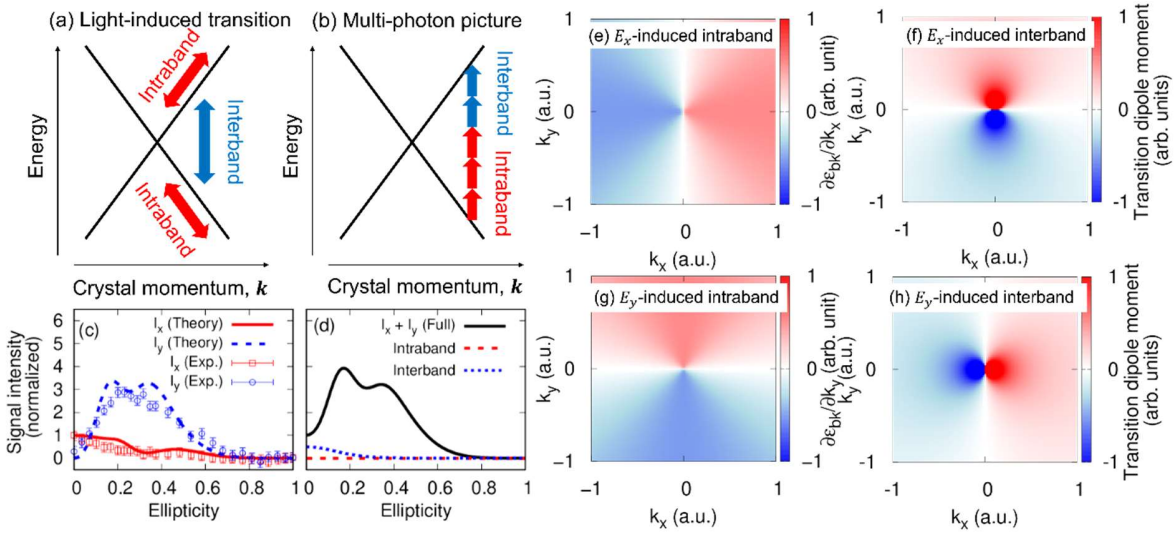

Figure 4. (a) Schematic diagram of Dirac-cone intraband and interband transitions. (b) Schematic multi-photon absorption process based on the combination of intraband and interband transitions. (c) Computed ellipticity dependence of HHG yield in graphene is shown by the solid and dashed curves from Ref. 44. Experimental results (data points including error bars) taken from Ref. 55 are shown for comparison. (d) Comparison of numerical results obtained using different calculation conditions. (e) Distribution of the magnitude of the intraband transitions induced by the x component of the electric field and (f) the corresponding distribution of the interband transitions. (g) Distribution of the magnitude of the intraband transitions induced by the y component of the

electric field and (h) the corresponding distribution of the interband transitions. Panels (e)–(h) are adapted from Ref. 47 under the Creative Commons Attribution 4.0 International license.

One possible way to manipulate the intraband motion in a band is to use multiple driving fields with different polarizations and different optical frequencies.[48] Figure 5a shows the excitation geometry that we used to study HHG in bulk GaSe (*c*-cut GaSe; thickness: 30 μm; bandgap energy: 2.0 eV). Here, we used two orthogonally polarized excitation pulses, defined by the electric fields $\boldsymbol{E_1}(t)$ and $\boldsymbol{E_2}(t)$ with photon energies $\hbar\omega_1 = 0.517$ eV and $\hbar\omega_2 = 0.954$ eV. The maximum electric field amplitudes inside the sample were $E_1 = 10$ MV/cm and $E_2 = 0.5$ MV/cm. Figure 5b plots the considered approximation of the potential of the first conduction band as a function of the two in-plane wavevectors k_x and k_y (we used a cosine-band approximation). The orientation of $\boldsymbol{E_1}(t)$ with respect to the crystal is expressed by the angle φ; $\varphi = 0$ is defined as the condition when $\boldsymbol{E_1}(t)$ is parallel to the zigzag direction of GaSe. The crystal-angle dependence of the HHG spectrum was measured by rotating the sample with respect to the *z*-axis. Figures 5c and 5d depict 2D maps of the φ dependences of the emitted high-order harmonics: Figure 5c shows the intensity of the emission polarized along the direction of $\boldsymbol{E_1}(t)$, I_1^{HH}, and Figure 5d shows that along the direction of $\boldsymbol{E_2}(t)$, I_2^{HH}. These maps reveal relatively complicated behavior: Firstly, peaks appear at photon energies equal to $m\hbar\omega_1+n\hbar\omega_2$, where *m* and *n* are integers that denote the harmonic order. Secondly, the even orders ($m + n$ = even) exhibit a six-fold rotational symmetry. For $m + n$ = even, I_1^{HH} vanishes at $\varphi = 30$ and 90°, while I_2^{HH} vanishes at $\varphi = 0$, 60, and 120°. The even orders (the peaks at $m\hbar\omega_1$ for m = even and the peaks at $n\hbar\omega_2$ for n = even) can be assigned to the components of the interband polarization, while the six-fold rotational symmetry of the harmonic orders obeying $m + n$ = even can be attributed to the conventional nonlinear polarization.

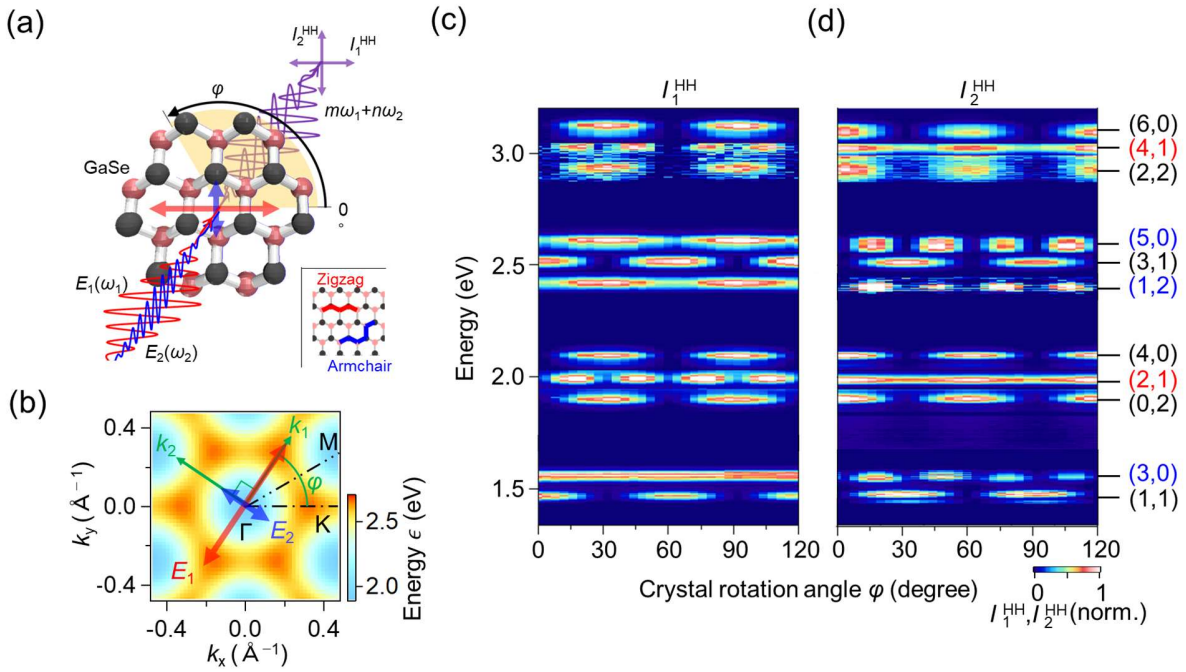

Figure 5. (a) Illustration of a GaSe crystal excited by two orthogonally polarized electric fields $\boldsymbol{E_1}(t)$ and $\boldsymbol{E_2}(t)$. (b) 2D map of the first conduction band based on a cosine approximation. (c) Component of the HHG spectrum that is polarized in the direction of $\boldsymbol{E_1}(t)$ as a function of the crystal angle, and (d) component that is polarized in the direction of $\boldsymbol{E_2}(t)$. The Panels in this figure are reproduced from Ref. 48 under a Creative Commons Attribution 4.0 International License.

On the other hand, the condition $m + n$ = odd results in either six- or twelve-fold rotational symmetries. For example, in the case of m = even, *i.e.*, (2,1) and (4,1), a twelve-fold rotational symmetry appears for I_1^{HH}. To explain this behavior, we consider that the two orthogonally polarized fields accelerate the electron along the two directions $\boldsymbol{k}_1$ and $\boldsymbol{k}_2$ of the conduction-band

potential shown in Figure 5b, which constitutes an intraband current. The electric field of the emitted harmonics can thus be separated into two mutually orthogonal harmonics, which are related to the band dispersion $\epsilon(\boldsymbol{k})$. The considered equation of motion is $d\boldsymbol{k}_i(t)/dt = -(e/\hbar)\boldsymbol{E}_i(t)$, where i = 1 and 2.[62] In the case of small E_1 and E_2 values, the response is isotropic because the electron stays in the convex potential region near the Γ point. If E_1 is increased, the electron is carried from the isotropic to the anisotropic region. Here, as the electron moves between the concave potential region and the convex region near the Γ point, the band curvature along $\boldsymbol{k}_2$ changes significantly, and thus dk_1/dt becomes larger than in the case of small E_1 values. Because the HHs are proportional to the time derivative of the band curvature, the intraband current amplitudes in both $\boldsymbol{k}$ directions are amplified by $\boldsymbol{E}_1$. Accordingly, since the conduction-band potential far away from the Γ point has a six-fold rotational symmetry, the harmonic intensities in the experiment show a six-fold rotational symmetry for E_1 around 10 MV/cm. In addition, the band structure possesses mirror symmetry about the axes defined by the Γ–K- and Γ–M-directions (the dashed dotted and the dashed double-dotted lines in Figure 5b), even far away from the Γ point, in addition to inversion symmetry with respect to the Γ point. Thus, when an electric field is applied along the Γ–K or Γ–M directions, the even oscillatory component of the current and the corresponding electric field of the emitted harmonic for the combinations (m, n) = (even, odd) and (odd, even) vanish. Therefore, these components become zero every 30° and show a twelve-fold rotational symmetry. These results show how the angular and polarization selection rules are governed by the order of the harmonics and the direction of the excitation field.

The polarization of the HHG spectrum can also be controlled by selecting a material with an appropriate topology. Here, we will briefly consider monolayer MoS_2,[63] which provides higher HHG efficiency than the bulk material does. The crystal structure of monolayer MoS_2 resembles

that of graphene and GaSe, because the atoms are arranged on a hexagonal crystal lattice. Similar to the analysis of HHG in GaSe, the experimental results can be represented on a 2D map where the harmonic intensity for a given order is plotted as a function of the angle between the polarization direction of the excitation light and a certain axis of the crystal. The crystal-angle dependence of the HHG spectrum of MoS_2 for excitation with a photon energy of 0.3 eV and a peak electric field of about 33 MV/cm reveals that the even harmonics are mainly polarized perpendicular to the excitation field. This result for the even harmonics has been attributed to transverse intraband currents induced by the Berry curvature. This type of current is referred to as anomalous current.

In conclusion, we provided an overview of the effects of intraband transitions in HHG. Firstly, we described how intraband transitions can be controlled by changing the quantum confinement in CdSe QDs. Secondly, to better illustrate this effect, we examined theoretical work on the coupling between intraband and interband transitions in graphene, where this coupling is responsible for a unique ellipticity dependence of the HHG yield. We note that ellipticity-induced HHG enhancements can be observed not only in graphene but also in bulk crystals including the archetypal direct-gap semiconductor GaAs.[65–68] These enhancements can be explained by interference between intraband and interband transition processes among multiple bands. On the other hand, it should also be considered that single- and multi-photon transitions, intraband transitions, and band-dressing can compete in the overall excitation process in multiband semiconductors such as germanium[32]. We consider that further research is needed to develop a complete microscopic theory of the interband and intraband transitions to thoroughly understand their role in the excitation processes related to HHG in solids.

Thirdly, we discussed two additional experiments on HHG: one examining the mechanism behind the angular and polarization selection rules of HHG in GaSe driven by two lasers, and another examining the unique polarization properties of HHG in MoS_2 related to the Berry curvature. The topology of the band structure can affect the currents responsible for HHG, and to exploit particular topological features of a given material, an appropriate driving field needs to be selected. While it was not discussed here, it has been shown that in three-dimensional topological insulators with band inversion, the spin–orbit interaction and time-reversal symmetry imply a connection between insulating bulk states and conducting surface states.[69–74] Regarding Bi_2Te_3,[69] a previous study showed that the surface states exhibit relatively high HHG efficiency, which was attributed to long scattering times caused by spin–momentum locking and a quasi-relativistic dispersion. Moreover, it was shown that the Berry curvature of Bi_2Te_3 affects the trajectories of the Dirac fermions, and this causes a unique polarization pattern in the emitted field.

We consider that the studies presented in this work provide insights into phenomena that are important for the realization of HHG-based solid-state devices (such as attosecond sources) and all-optical reconstruction of the band structure. Note that attosecond emissions from a solid target (silicon dioxide) has already been reported,[23] but the required bias-field strength (110 MV/cm) may be too high for broad application. Metallic nanostructures and dielectric metasurfaces may help to resolve this issue.[75–82] To realize petahertz devices, which are electronic devices that operate in the petahertz regime (instead of the gigahertz regime), suitable light sources are needed, as well as measures to reduce power consumption. One such measure would be to efficiently focus the high-order harmonic emission, which can be achieved by using nano-structured devices.[83] To keep the broader context in mind, we would like to end by noting that, so far, much research has been performed using intense electric fields, but recently it has also become possible to generate

high-intensity magnetic field pulses, which will enable new nonlinear effects to be studied.[84–88] The effects presented in this article could be exploited in the development of unique technologies that will push operation speeds beyond the gigahertz regime while still being compatible with today's semiconductor technology.

ASSOCIATED CONTENT

Supporting Information

The Supporting Information is available free of charge at

Microscopic theory of HHG in solids

AUTHOR INFORMATION

Corresponding Authors

Hideki Hirori − Institute for Chemical Research, Kyoto University, Uji, Kyoto 611-0011, Japan; orcid.org/0000-0001-6056-8675; Email: hirori@scl.kyoto-u.ac.jp

Shunsuke A. Sato − Center for Computational Sciences, University of Tsukuba, Tsukuba 305-8577, Japan; Max Planck Institute for the Structure and Dynamics of Matter, Luruper Chaussee 149, 22761 Hamburg, Germany; orcid.org/0000-0001-9543-2620; Email: ssato@ccs.tsukuba.ac.jp

Yoshihiko Kanemitsu − Institute for Chemical Research, Kyoto University, Uji, Kyoto 611-0011, Japan; orcid.org/0000-0002-0788-131X; Email: kanemitu@scl.kyoto-u.ac.jp

Notes

The authors declare no competing financial interest.

Biographies

Hideki Hirori received his PhD degree in physics from Kyoto University in 2006. He is an Associate Professor of Physics at the Institute for Chemical Research, Kyoto University. His research interests include strong-field light-matter interaction in semiconductors and control elementary dynamics in quantum nano materials.

Shunsuke A. Sato received his PhD degree in physics from University of Tsukuba in 2016. He is an Assistant Professor at University of Tsukuba. His research interests include attosecond physics of solid-state systems and computational physics for electron dynamics.

Yoshihiko Kanemitsu received his PhD from The University of Tokyo in 1986. He is a Professor of Physics at the Institute for Chemical Research, Kyoto University. His research interests include exciton physics of nanocrystal quantum dots and nonlinear optics of semiconductors under extremely strong electric fields.

ACKNOWLEDGMENTS

The authors would like to thank many colleagues for their contributions and useful discussions. In particular, the authors gratefully acknowledge K. Nakagawa and Y. Sanari and T. Yamada for their support. Part of this study was supported by a grant from the Japan Society for the Promotion of Science (JSPS KAKENHI Grant No. JP19H05465). HH acknowledges the financial support of the Japan Society for the Promotion of Science (JSPS KAKENHI Grant No. JP21H01842).

References

(1) Boyd, R. W. Nonlinear Optics, 3rd ed; Academic Press, **2008**.

(2) Franken, P. A.; Hill, A. E.; Peters, C. W.; Weinreich, G. Generation of optical harmonics.

Phys. Rev. Lett. **1961**, *7*, 118–119. DOI: 10.1103/PhysRevLett.7.118

(3) Ferray, M.; L'Huillier, A.; Li, X. F.; Lompre, L. A.; Mainfray, G.; Manus, C. Multiple-harmonic conversion of 1064 nm radiation in rare gases. *J. Phys. B: At. Mol. Opt. Phys*. **1988**, *21*, L31–L35. DOI: 10.1088/0953-4075/21/3/001

(4) Hentschel, M.; Kienberger, R.; Spielmann, Ch.; Reider, G. A.; Milosevic, N.; Brabec, T.; Corkum, P.; Heinzmann, U.; Drescher M.; Krausz, F. Attosecond metrology. *Nature* **2001**, *414*, 509–513. DOI: 10.1038/35107000

(5) Paul, P. M.; Toma, E. S.; Breger, P.; Mullot, G.; Augé, F.; Balcou, Ph.; Muller, H. G.; Agostini, P. Observation of a train of attosecond pulses from high harmonic generation. *Science* **2001**, *292*, 1689–1692. DOI: 10.1126/science.1059413

(6) Corkum, P. B.; Krausz, F. Attosecond science. *Nat. Phys*. **2007**, *3*, 381–387. DOI: 10.1038/nphys620

(7) Kaindl, R. A.; Wurm, M.; Reimann, K.; Hamm P.; Weiner A. M.; Woerner M. Generation, shaping, and characterization of intense femtosecond pulses tunable from 3 to 20 μm. *J. Opt. Soc. Am. B* **2000**, *17*, 2086–2094. DOI: 10.1364/JOSAB.17.002086

(8) Hebling, J.; Almási, G.; Kozma, I. Z.; Kuhl, J. Velocity matching by pulse front tilting for large-area THz-pulse generation. *Opt. Express* **2002**, *10*, 1161–1166. DOI: 10.1364/OE.10.001161

(9) Zentgraf, T.; Huber, R.; Nielsen, N. C.; Chemla, D. S.; Kaindl, R. A. Ultrabroadband 50-130 THz pulses generated via phase-matched difference frequency mixing in $LiIO_3$. *Opt. Express* **2007**, *15*, 5775–5781. DOI: 10.1364/OE.15.005775

(10) Yeh, K. L.; Hoffmann, M. C.; Hebling, J.; Nelson, K. A. Generation of 10 μJ ultrashort terahertz pulses by optical rectification. *Appl. Phys. Lett.* **2007**, *90*, 171121. DOI: 10.1063/1.2734374

(11) Sell, A.; Leitenstorfer, A.; Huber, R. Phase-locked generation and field-resolved detection of widely tunable terahertz pulses with amplitudes exceeding 100 MV/cm. *Opt. Lett*. **2008**, *33*, 2767–2769. DOI: 10.1364/OL.33.002767

(12) Brida, D.; Marangoni, M.; Manzoni, C.; De Silvestri, S.; Cerullo, G. Two-optical-cycle pulses in the mid-infrared from an optical parametric amplifier. *Opt. Lett*. **2008**, *33*, 2901–2903. DOI: 10.1364/OL.33.002901

(13) Hirori, H.; Doi, A.; Blanchard, F.; Tanaka, K. Single-cycle terahertz pulses with amplitudes

exceeding 1 MV/cm generated by optical rectification in $LiNbO_3$. *Appl. Phys. Lett.* **2011**, *98*, 091106. DOI: 10.1063/1.3560062

(14) Sanari, Y.; Sekiguchi, F.; Nakagawa, K.; Ishii, N.; Kanemitsu, Y.; Hirori, H. Generation of wavelength-tunable few-cycle pulses in the mid-infrared at repetition rates up to 10 kHz. *Opt. Lett.* **2021**, *46*, 5280–5283. DOI: 10.1364/OL.440228

(15) Kanda, N.; Ishii, N.; Itatani, J.; Matsunaga, R. Optical parametric amplification of phase-stable terahertz-to-mid-infrared pulses studied in the time domain. *Opt. Express* **2021**, *29*, 3479–3489. DOI: 10.1364/OE.413200

(16) Dalla-Barba G.; Jargot, G.; Lassonde, P.; Tóth, S.; Haddad, E.;Boschini, F.; Delagnes, J.-C.; Leblanc, A.; Ibrahim, H.; Cormier, E.; Légaré, F. Mid-infrared frequency domain optical parametric amplifier. *Opt. Express* **2023**, *31*, 14954–14964. DOI: 10.1364/OE.487813

(17) Chin, A. H.; Calderón, O. G.; Kono, J. Extreme midinfrared nonlinear optics in semiconductors. *Phys. Rev. Lett.* **2001**, *86*, 3292–3295. DOI: 10.1103/PhysRevLett.86.3292

(18) Ghimire, S.; DiChiara, A. D.; Sistrunk, E.; Agostini, P.; DiMauro, L. F; Reis, D. A. Observation of high-order harmonic generation in a bulk crystal. *Nat. Phys*. **2011**, *7*, 138–141. DOI: 10.1038/NPHYS1847

(19) Schubert, O.; Hohenleutner, M.; Langer, F.; Urbanek, B.; Lange, C.; Huttner, U.; Golde, D.; Meier, T.; Kira, M.; Koch, S. W.; Huber, R. Sub-cycle control of terahertz high-harmonic generation by dynamical Bloch oscillations. *Nat. Photon.* **2014**, *8*, 119–123. DOI: 10.1038/NPHOTON.2013.349

(20) Luu, T. T.; Garg, M.; Kruchinin, S. Y.; Moulet, A.; Hassan, M. Th.; Goulielmakis, E. Extreme ultraviolet high-harmonic spectroscopy of solids. *Nature* **2015**, *521*, 498–502. DOI: 10.1038/nature14456

(21) Vampa, G.; Hammond, T. J.; Thiré, N.; Schmidt, B. E.; Légaré, F.; McDonald, C. R.; Brabec, T.; Corkum, P. B. Linking high harmonics from gases and solids. *Nature* **2015**, *522*, 462–464. DOI: 10.1038/nature14517

(22) Hohenleutner, M.; Langer, F.; Schubert, O.; Knorr, M.; Huttner, U.; Koch, S. W.; Kira, M.; Huber, R. Real-time observation of interfering crystal electrons in high-harmonic generation. *Nature* **2015**, *523*, 572–575. DOI: 10.1038/nature14652

(23) Garg, M.; Zhan, M.; Luu, T. T.; Lakhotia, H.; Klostermann, T.; Guggenmos, A.; Goulielmakis, E. Multi-petahertz electronic metrology. *Nature* **2016**, *538*, 359–363. DOI:

10.1038/nature19821

(24) Ndabashimiye, G.; Ghimire, S.; Wu, M.; Browne, D. A.; Schafer, K. J.; Gaarde, M. B.; Reis, D. A. Solid-state harmonics beyond the atomic limit. *Nature* **2016**, *534*, 520–523. DOI: 10.1038/nature17660

(25) Corkum, P. B. Plasma perspective on strong field multiphoton ionization. *Phys. Rev. Lett*. **1993**, *71*, 1994–1997. DOI: 10.1103/PhysRevLett.71.1994

(26) Kulander, K. C.; Schafer, K. J.; Krause, J. L. Dynamics of Short-Pulse Excitation, Ionization and Harmonic Conversion. Proceedings of a NATO Advanced Research Workshop on SILAP (Super-Intense Laser-Atom Physics), Piraux, B.; L'Huillier, A.; Rzazewski, K. (Eds.), Plenum Press: New York, **1993**, *316*, 95–110.

(27) Schafer, K.J.; Yang, B.; DiMauro, L. F.; Kulander, K. C. Above threshold ionization beyond the high harmonic cutoff. *Phys. Rev. Lett.* **1993**, *70*, 1599–1602. DOI: 10.1103/PhysRevLett.70.1599

(28) Golde, D.; Meier, T.; Koch, S. W. High harmonics generated in semiconductor nanostructures by the coupled dynamics of optical inter- and intraband excitations. *Phys. Rev. B* **2008**, *77*, 075330. DOI: 10.1103/PhysRevB.77.075330

(29) Vampa, G.; McDonald, C. R.; Orlando, G.; Klug, D. D.; Corkum, P. B.; Brabec, T. Theoretical analysis of high-harmonic generation in solids. *Phys. Rev. Lett.* **2014**, *113*, 073901. DOI:10.1103/PhysRevLett.113.073901

(30) Sato, S. A.; Lucchini, M.; Volkov, M.; Schlaepfer, F.; Gallmann, L.; Keller, U.; Rubio, A. Role of intraband transitions in photocarrier generation. *Phys. Rev. B* **2018**, *98*, 035202. DOI: 10.1103/PhysRevB.98.035202

(31) Schlaepfer, F.; Lucchini, M.; Sato, S. A.; Volkov, M.; Kasmi, L.; Hartmann, N.; Rubio, A.; Gallmann, L.; Keller, U. Attosecond optical-field-enhanced carrier injection into the GaAs conduction band. *Nat. Phys.* **2018**, *14*, 560–564. DOI: 10.1038/s41567-018-0069-0

(32) Inzani, G.; Adamska, L.; Eskandari-asl, A.; Di Palo, N.; Dolso, G. L.; Moio, B.; D'Onofrio, L. J.; Lamperti, A.; Molle, A.; Borrego-Varillas, R.; Nisoli, M.; Pittalis, S.; Rozzi, C. A.; Avella, A.; Lucchini, M. Field-driven attosecond charge dynamics in germanium. *Nat. Photon.* **2023**, *17*, 1059–1065. DOI: 10.1038/s41566-023-01274-1

(33) Kuehn, W.; Gaal, P.: Reimann, K.; Woerner, M.; Elsaesser, T.; Hey, R. Coherent ballistic motion of electrons in a periodic potential. *Phys. Rev. Lett.* **2010**, *104*, 146602. DOI:

10.1103/PhysRevLett.104.146602

(34) Vampa, G.; Hammond, T. J.; Thiré, N.; Schmidt, B. E.; Légaré, F.; McDonald, C. R.; Brabec, T.; Klug, D. D.; Corkum, P. B. All-optical reconstruction of crystal band structure. *Phys. Rev. Lett.* **2015**, *115*, 193603. DOI:10.1103/PhysRevLett.115.193603

(35) Borsch, M.; Schmid, C. P.; Weigl, L.; Schlauderer, S.; Hofmann, N.; Lange, C.; Steiner, J. T.; Koch, S. W.; Huber, R.; Kira, M. Super-resolution lightwave tomography of electronic bands in quantum materials. *Science* **2020**, *370*, 1204–1207. DOI: 10.1126/science.abe2112

(36) Lakhotia, H.; Kim, H. Y.; Zhan, M.; Hu, S.; Meng, S.; Goulielmakis, E. Laser picoscopy of valence electrons in solids. *Nature* **2020**, *583*, 55–59. DOI: 10.1038/s41586-020-2429-z

(37) Cundiff, S. T.; Knorr, A.; Feldmann, J.; Koch, S. W.; Göbel, E. O.; Nickel, H. Rabi flopping in semiconductors. *Phys. Rev. Lett*. **1994**, *73*, 1178–1181. DOI: 10.1103/PhysRevLett.73.1178

(38) Mücke, O. D.; Tritschler, T; Wegener, M.; Morgner, U.; Kärtner, F. X. Role of the carrier-envelope offset phase of few-cycle pulses in nonperturbative resonant nonlinear optics. *Phys. Rev. Lett.* **2002**, *89*, 127401. DOI: 10.1103/PhysRevLett.89.127401

(39) Goulielmakis, E.; Yakovlev, V. S.; Cavalieri, A. L.; Uiberacker, M.; Pervak, V.; Apolonski, A.; Kienberger, R.; Kleineberg, U.; Krausz, F. Attosecond control and measurement: lightwave electronics. *Science* **2007**, *317*, 769–775. DOI:10.1126/science.1142855

(40) Schultze, M.; Bothschafter, E. M.; Sommer, A.; Holzner, S.; Schweinberger, W.; Fiess, M.; Hofstetter, M.; Kienberger, R.; Apalkov, V.; Yakovlev, V. S.; Stockman, M. I.; Krausz, F. Controlling dielectrics with the electric field of light. *Nature* **2013**, *493*, 75–78. DOI: 10.1038/nature11720

(41) Schiffrin, A.; Paasch-Colberg, T.; Karpowicz, N.; Apalkov, V.; Gerster, D.; Mühlbrandt, S.; Korbman, M.; Reichert, J.; Schultze, M.; Holzner, S.; Barth, J. V.; Kienberger, R.; Ernstorfer, R.; Yakovlev, V. S.; Stockman, M. I.; Krausz, F. Optical-field-induced current in dielectrics. *Nature* **2013**, *493*, 70–74. DOI:10.1038/nature11567

(42) Higuchi, T.; Heide, C.; Ullmann, K.; Weber, H. B.; Hommelhoff, P. Light-field-driven currents in graphene. *Nature* **2017**, *550*, 224–228. DOI:10.1038/nature23900

(43) Boolakee, T.; Heide, C.; Garzón-Ramírez, A.; Weber, H. B.; Franco, I.; Hommelhoff, P. Light-field control of real and virtual charge carriers. *Nature* **2022**, *605*, 251–255. DOI: 10.1038/s41586-022-04565-9

(44) Yoshioka, K.; Wakamura, T.; Hashisaka, M.; Watanabe, K.; Taniguchi, T.; Kumada, N. Ultrafast intrinsic optical-to-electrical conversion dynamics in a graphene photodetector. *Nat. Photon.* **2022**, *16*, 718–723. DOI:10.1038/s41566-022-01058-z

(45) Nakagawa, K.; Hirori, H.; Sanari, Y.; Sekiguchi, F.; Sato, R.; Saruyama, M.; Teranishi, T.; Kanemitsu, Y. Interference effects in high-order harmonics from colloidal perovskite nanocrystals excited by an elliptically polarized laser. *Phys. Rev. Materials* **2021**, *5*, 016001 DOI: 10.1103/PhysRevMaterials.5.016001

(46) Nakagawa, K.; Hirori, H.; Sato, S. A.; Tahara, H.; Sekiguchi, F.; Yumoto, G.; Saruyama, M.; Sato, R.; Teranishi, T.; Kanemitsu, Y. Size-controlled quantum dots reveal the impact of intraband transitions on high-order harmonic generation in solids. *Nat. Phys.* **2022**, *18*, 874–878. DOI:10.1038/s41567-022-01639-3

(47) Sato, S. A.; Hirori, H.; Sanari, Y.; Kanemitsu, Y.; Rubio, A. High-order harmonic generation in graphene: Nonlinear coupling of intraband and interband transitions. *Phys. Rev. B* **2021**, *103*, L041408. DOI:10.1103/PhysRevB.103.L041408

(48) Sanari, Y.; Otobe, T.; Kanemitsu, Y.; Hirori, H. Modifying angular and polarization selection rules of high-order harmonics by controlling electron trajectories in k-space. *Nat. Commun.* **2020**, *11*, 3069. DOI:10.1038/s41467-020-16875-5

(49) Hirori, H.; Xia, P.; Shinohara, Y.; Otobe, T.; Sanari, Y.; Tahara, H.; Ishii, N.; Itatani, J.; Ishikawa, K. L.; Aharen, T.; Ozaki, M.; Wakamiya, A.; Kanemitsu, Y. High-order harmonic generation from hybrid organic–inorganic perovskite thin films. *APL Mater.* **2019**, *7*, 041107. DOI: 10.1063/1.5090935

(50) Sanari, Y.; Hirori, H.; Aharen, T.; Tahara, H.; Shinohara, Y.; Ishikawa, K. L.; Otobe, T.; Xia, P.; Ishii, N.; Itatani, J.; Sato, S. A.; Kanemitsu, Y. Role of virtual band population for high harmonic generation in solids. *Phys. Rev. B* **2020**, *102*, 041125. DOI:10.1103/PhysRevB.102.041125

(51) Jürgens, P.; Liewehr, B.; Kruse; B.; Peltz, C.; Engel, D.; Husakou, A.; Witting, T.; Ivanov, M.; Vrakking, M. J. J.; Fennel, T.; Mermillod-Blondin, A. Origin of strong-field-induced low-order harmonic generation in amorphous quartz. *Nat. Phys.* **2020**, *16*, 1035–1039. DOI: 10.1038/s41567-020-0943-4

(52) Efros, Al. L.; Efros, A. L. Interband absorption of light in a semiconductor sphere. *Sov. Phys. Semicond.* **1982**, *16*, 772–775.

(53) Brus, L. E. A simple model for the ionization potential, electron affinity, and aqueous redox potentials of small semiconductor crystallites. *J. Chem. Phys.* **1983**, *79*, 5566–5571. DOI: 10.1063/1.445676

(54) Ekimov, A. I.; Hache, F.; Schanne-Klein, M. C.; Ricard, D.; Flytzanis, C.; Kudryavtsev, I. A.; Yazeva, T. V.; Rodina, A. V.; Efros, A. L. Absorption and intensity-dependent photoluminescence measurements on CdSe quantum dots: assignment of the first electronic transitions. *J. Opt. Soc. Am. B* **1993**, *10*, 100–107. DOI:10.1364/JOSAB.10.000100

(55) Murray, C. B.; Norris, D. J.; Bawendi, M. G. Synthesis and characterization of nearly monodisperse CdE (E=S,Se,Te) semiconductor nanocrystallites. *J. Am. Chem. Soc.* **1993**, *115*, 8706–8715. DOI:10.1021/ja00072a025

(56) McDonald, C. R.; Amin, K. S.; Aalmalki, S.; Brabec, T. Enhancing high harmonic output in solids through quantum confinement. *Phys. Rev. Lett.* **2017**, *119*, 183902. DOI: 10.1103/PhysRevLett.119.183902

(57) Gopalakrishna, H. N.; Baruah, R.; Hünecke, C.; Korolev, V.; Thuemmler, M.; Croy, A.; Richter, M.; Yahyaei, F.; Hollinger, R.; Shumakova, V.; Uschmann, I.; Marschner, H.; Zuerch, M.; Reichardt, C.; Undisz, A.; Dellith, J.; Pugzlys, A.; Baltuska, A.; Spielmann, C.; Peschel, U.; Graefe, S.; Waechtler, M.; Kartashov, D. Tracing spatial confinement in semiconductor quantum dots by high-order harmonic generation, *Phys. Rev. Research* **2023**, *5*, 013128, DOI: 10.1103/PhysRevResearch.5.013128

(58) Yoshikawa, N.; Tamaya, T.; Tanaka, K. High-harmonic generation in graphene enhanced by elliptically polarized light excitation. *Science* **2017**, *356*, 736–738. DOI: 10.1126/science.aam8861

(59) Geim, A. K. Graphene: Status and prospects. *Science* **2009**, *324*, 1530–1534. DOI: 10.1126/science.1158877

(60) Hafez, H. A.; Kovalev, S.; Deinert, J. C.; Mics, Z.; Green, B.; Awari, N.; Chen, M.; Germanskiy, S.; Lehnert, U.; Teichert, J.; Wang, Z.; Tielrooij, K. J.; Liu, Z.; Chen, Z.; Narita, A.; Müllen, K.; Bonn, M.; Gensch, M.; Turchinovich, D. Extremely efficient terahertz high-harmonic generation in graphene by hot Dirac fermions. *Nature* **2018**, *561*, 507–511. DOI:10.1038/s41586-018-0508-1

(61) Cha, S.; Kim, M.; Kim, Y.; Choi, S.; Kang, S.; Kim, H.; Yoon, S.; Moon, G.; Kim, T.; Lee, Y. W.; Cho, G. Y.; Park, M. J.; Kim, C.-J.; Kim, B. J.; Lee, J.-D.; Jo, M.-H.; Kim, J. Gate-

tunable quantum pathways of high harmonic generation in graphene, *Nat Commun.* **2022**, *13*, 6630. DOI:10.1038/s41467-022-34337-y

(62) Kaneshima, K.; Shinohara, Y.; Takeuchi, K.; Ishii, N.; Imasaka, K.; Kaji, T.; Ashihara, S.; Ishikawa, K. L.; Itatani, J. Polarization-resolved study of high harmonics from bulk semiconductors. *Phys. Rev. Lett.* **2018**, *120*, 243903. DOI:10.1103/PhysRevLett.120.243903

(63) Liu, H.; Li, Y.; You, Y. S.; Ghimire, S.; Heinz, T. F.; Reis, D. A. High-harmonic generation from an atomically thin semiconductor. *Nat. Phys.* **2016**, *13*, 262–265. DOI:10.1038/NPHYS3946

(64) Tancogne-Dejean, N.; Mücke, O. D.; Kärtner, F. X.; Rubio, A. Ellipticity dependence of high-harmonic generation in solids originating from coupled intraband and interband dynamics. *Nat. Commun.* **2017**, *8*, 745. DOI: 10.1038/s41467-017-00764-5

(65) You, Y. S.; Reis, D., A.; Ghimire, S. Anisotropic high-harmonic generation in bulk crystals. *Nat. Phys.* **2017**, *13*, 345–349. DOI: 10.1038/nphys3955

(66) Xiao, D.; Chang, M.-C.; Niu, Q. Berry phase effects on electronic properties. *Rev. Mod. Phys.* **2010**, *82*, 1959–2007. DOI: 10.1103/RevModPhys.82.1959

(67) Sekiguchi, F.; Sakamoto, M.; Nakagawa, K.; Tahara, H.; Sato, S. A.; Hirori, H.; Kanemitsu, Y. Enhancing high harmonic generation in GaAs by elliptically polarized light excitation. *Phys. Rev. B* **2023**, 108, 205201. DOI: 10.1103/PhysRevB.108.205201

(68) Sekiguchi, F.; Yumoto, G.; Hirori, H.; Kanemitsu, Y. Polarization anomaly in high harmonics in the crossover region between perturbative and extreme nonlinearity in GaAs. *Phys. Rev. B* **2022**, *106*, L241201. DOI:10.1103/PhysRevB.106.L241201

(69) Schmid, C. P.; Weigl, L.; Grössing, P.; Junk, V; Gorini, C.; Schlauderer, S.; Ito, S.; Meierhofer, M.; Hofmann, N.; Afanasiev, D.; Crewse, J.; Kokh, K. A.; Tereshchenko, O. E.; Güdde, J.; Evers, F.; Wilhelm, J.; Richter, K.; Höfer, U.; Huber, R. Tunable non-integer high-harmonic generation in a topological insulator. *Nature* **2021**, *593*, 385–390. DOI:10.1038/s41586-021-03466-7

(70) Bai, Y.; Fei, F. C.; Wang, S.; Li, N.; Li, X.; Song, F.; Li, R.; Xu, Z.; Liu, P. High-harmonic generation from topological surface states. *Nat. Phys.* **2021**, *17*, 311–315. DOI:10.1038/s41567-020-01052-8

(71) Baykusheva, D.; Chacón, A.; Lu, J.; Bailey, T. P.; Sobota, J. A.; Soifer, H.; Kirchmann, P. S.; Rotundu, C.; Uher, C.; Heinz, T. F.; Reis, D. A.; Ghimire, S. All-optical probe of three-

dimensional topological insulators based on high-harmonic generation by circularly polarized laser fields. *Nano Lett.* **2021**, *21*, 8970–8978. DOI: 10.1021/acs.nanolett.1c02145

(72) Heide, C.; Kobayashi, Y.; Baykusheva, D. R.; Jain, D.; Sobota, J. A.; Hashimoto, M.; Kirchmann, P. S.; Oh, S.; Heinz, T. F.; Reis, D. A.; Ghimire, S. Probing Topological phase transitions using high-harmonic generation. *Nat. Photon.* **2022**, *16*, 620–624. DOI: 10.1038/s41566-022-01050-7

(73) Cheng, B.; Kanda, N.; Ikeda, T. N..; Matsuda, T.; Xia, P.; Schumann, T.; Stemmer, S.; Itatani, J.; Armitage, N. P.; Matsunaga, R. Efficient terahertz harmonic generation with coherent acceleration of electrons in the Dirac semimetal Cd_3As_2. *Phys. Rev. Lett.* **2020**, *124*, 117402. DOI:10.1103/PhysRevLett.124.117402

(74) Kovalev, S.; Dantas, R. M. A.; Germanskiy, S.; Deinert, J. C.; Green, B.; Ilyakov, I.; Awari, N.; Chen, M.; Bawatna, M.; Ling, J.; Xiu, F.; van Loosdrecht, P. H. M.; Surówka, P.; Oka, T.; Wang, Z. Non-perturbative terahertz high-harmonic generation in the three-dimensional Dirac semimetal Cd_3As_2. *Nat. Commun.* **2020**, *11*, 2451. DOI:10.1038/s41467-020-16133-8

(75) Cocker, T. L.; Jelic, V.; Gupta, M.; Molesky, S. J.; Burgess, J. A. J.; De Los Reyes, G.; Titova, L. V.; Tsui, Y. Y.; Freeman, M. R.; Hegmann, F. A. An ultrafast terahertz scanning tunnelling microscope. *Nat. Photon.* **2013**, *7*, 620–625. DOI:10.1038/NPHOTON.2013.151

(76) Cocker, T. L.; Peller, D.; Yu, P.; Repp, J.; Huber, R. Tracking the ultrafast motion of a single molecule by femtosecond orbital imaging. *Nature* **2016**, *539*, 263–267. DOI:10.1038/nature19816

(77) Vampa, G.; Ghamsari, B. G.; Mousavi, S. S.; Hammond, T. J.; Olivieri, A.; Lisicka-Skrek, E.; Naumov, A. Y.; Villeneuve, D. M.; Staudte, A.; Berini, P.; Corkum, P. B. Plasmon-enhanced high-harmonic generation from silicon. *Nat. Phys.* **2017**, *13*, 659–662. DOI:10.1038/NPHYS4087

(78) Imasaka, K.; Kaji, T.; Shimura, T.; Ashihara, S. Antenna-enhanced high harmonic generation in a wide-bandgap semiconductor ZnO. *Opt. Express* **2018**, *26*, 21364–21374. DOI:10.1364/OE.26.021364

(79) Du, S.; Yoshida, K.; Zhang, Y.; Hamada, I.; Hirakawa, K. Terahertz dynamics of electron–vibron coupling in single molecules with tunable electrostatic potential. *Nat. Photon.* **2018**, *12*, 608–612. DOI:10.1038/s41566-018-0241-1

(80) Ludwig, M.; Aguirregabiria, G.; Ritzkowsky, F.; Rybka, T.; Marinica, D. C.; Aizpurua, J.;

Borisov, A. G.; Leitenstorfer, A.; Brida, D. Sub-femtosecond electron transport in a nanoscale gap. *Nat. Phys.* **2020**, *16*, 341–345. DOI:10.1038/s41567-019-0745-8

(81) Yoshida, S.; Arashida, Y.; Hirori, H.; Tachizaki, T.; Taninaka, A.; Ueno, H.; Takeuchi, O.; Shigekawa, H. Terahertz scanning tunneling microscopy for visualizing ultrafast electron motion in nanoscale potential variations. *ACS Photon.* **2021**, *8*, 315–323. DOI:10.1021/acsphotonics.0c01572

(82) Liu, H.; Guo, C.; Vampa, G.; Zhang, J. L.; Sarmiento, T.; Xiao, M.; Bucksbaum, P. H.; Vuckovic, J.; Fan, S.; Reis, D. A. Enhanced high-harmonic generation from an all-dielectric metasurface. *Nat. Phys.* **2018**, *14*, 1006–1010. DOI:10.1038/s41567-018-0233-6

(83) Sivis, M.; Taucer, M.; Vampa, G.; Johnston, K.; Staudte, A.; Naumov, A. Y.; Villeneuve, D. M.; Ropers, C.; Corkum, P. B. Tailored semiconductors for high-harmonic optoelectronics. *Science* **2017**, *357*, 303–306. DOI:10.1126/science.aan2395

(84) Kampfrath, T.; Sell, A.; Klatt, G.; Pashkin, A.; Mährlein, S.; Dekorsy, T.; Wolf, M.; Fiebig, M.; Leitenstorfer, A.; Huber, R. Coherent terahertz control of antiferromagnetic spin waves. *Nat. Photon.* **2011**, *5*, 31–34. DOI:10.1038/NPHOTON.2010.259

(85) Mukai, Y.; Hirori, H; Yamamoto, T.; Kageyama, H.; Tanaka, K. Nonlinear magnetization dynamics of antiferromagnetic spin resonance induced by intense terahertz magnetic field. *New J. Phys.* **2016,** *18*, 013045. DOI:10.1088/1367-2630/18/1/013045

(86) Schlauderer, S.; Lange, C.; Baierl, S.; Ebnet, T.; Schmid, C. P.; Valovcin, D. C.; Zvezdin, A. K.; Kimel, A. V.; Mikhaylovskiy, R. V.; Huber, R. Temporal and spectral fingerprints of ultrafast all-coherent spin switching. *Nature* **2019**, *569*, 383–387. DOI:10.1038/s41586-019-1174-7

(87) Mashkovich, E. A.; Grishunin, K. A.; Dubrovin, R. M.; Zvezdin, A. K.; Pisarev, R. V.; Kimel, A. V. Terahertz-light driven coupling of antiferromagnetic spins to lattice. *Science* **2021**, *374*, 1608–1611. DOI:10.1126/science.abk1121

(88) Zhang, Z.; Sekiguchi, F.; Moriyama, T.; Furuya, S. C.; Sato, M.; Satoh, T.; Mukai, Y.; Tanaka, K.; Yamamoto, T.; Kageyama, H.; Kanemitsu, Y.; Hirori, H. Generation of third-harmonic spin oscillation from strong spin precession induced by terahertz magnetic near fields. *Nat. Commun.* **2023**, *14*, 1795. DOI:10.1038/s41467-023-37473-1z